Materials & Design 216 (2022) 110559

Contents lists available at ScienceDirect

Materials & Design

journal homepage: www.elsevier.com/locate/matdes

# Insertion of large diameter through-thickness metallic pins in composites

Geoffrey Neale *, Alex Skordos

*Enhanced Composites and Structures Centre, Cranfield University, Wharley End, Bedford MK43 0AL, UK*

## HIGHLIGHTS

- New method for insertion of large diameter pins in prepreg composite laminates.
- Conical leading-edge pins exhibit low insertion force with better insertion quality.
- Insertion forces increase exponentially with pin diameter.
- Prepreg stack consolidation improves insertion quality by reducing tow distortions.

## GRAPHICAL ABSTRACT

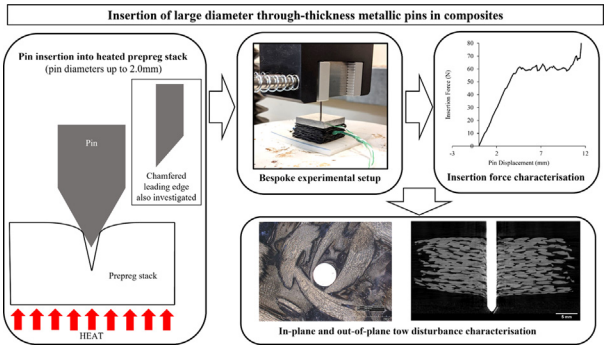


## ARTICLE INFO

*Article history:*
Received 13 December 2021
Revised 8 March 2022
Accepted 14 March 2022
Available online 16 March 2022

*Keywords:*
Prepreg processing
Damage mechanics
Thermal analysis
Tow

## ABSTRACT

Existing Through-Thickness Reinforcement (TTR) methods for laminated composites using semi or fully rigid reinforcing elements, like tufting, stitching, and z-pinning, present limitations on reinforcing element geometry, strength, and stiffness. Where these application envelopes are exceeded, TTR element insertion results in unacceptable levels of damage to both the composite and/or TTR elements. Here, we demonstrate that low-speed insertion of rigid reinforcements into heated prepreg preforms is a feasible and robust reinforcement process capable of providing accurate TTR element placement with minimal tow disturbance compared with existing methods for similar pin sizes. The insertion process is characterised with respect to insertion forces, and mesoscale laminate deformation/damage for carbon-benzoxazine prepreg preforms. The research investigates the influence of pin leading edge on insertion for a range of pin diameters (1.2, 1.5, and 2.0 mm) and preform consolidation states, describing low insertion forces and good quality laminate preforms. Insertion forces increase with pin diameter, typically resulting from increased pin-tow contact area and friction. Large diameter sizes and low insertion forces expand the range and forms of materials that can be inserted compared to existing TTR methods and show that this method can potentially be transferred to benefit work on composite hole creation, joining, and repair.



## 1. Introduction

There is an increasing demand for the use of functional through-thickness reinforcement (TTR) in composites in line with the uptake of composite materials in more non-traditional industries and applications [1]. A variety of through-thickness reinforcement (TTR) methods in composites are regularly used, although primarily to improve delamination resistance [2,3], for the integration of functional elements into composites that can add thermal/-electrical management [4–7], sensing [8] and joining functionalities [9–11] to composite materials. However, existing

* Corresponding author.
*E-mail address:* g.d.neale@cranfield.ac.uk (G. Neale).

https://doi.org/10.1016/j.matdes.2022.110559
0264-1275/

TTR methods like tufting, stitching, and z-pinning, place strict limitations on the properties of the reinforcing elements [12,13].

In the case of tufting, tows/wire/filaments must be strong yet flexible enough to sustain the small bending radii endured during tufting [14]. In stitching, similar constraints are present with the added constraint that tows must be knotted on the underside, in some cases requiring access to both sides of the preform [12], but one-sided stitching techniques can be employed. In both processes, only dry fibre preforms are typically suitable media for the integration of TTR, with tufting having a limited envelope of applicability in prepregs. Z-pinning offers a system for the integration of rigid elements through prepregs where an array of rigid pins is inserted into prepreg stacks with the assistance of ultrasonic impactor [13,15]. Pins are typically metallic, polymeric, or composite to achieve the desired stiffness and are quite small (0.2 to 1.0 mm diameters). A low vol.% (0.5–4 vol%) array of pins is used to generate the TTR improvements [16] which has a more positive impact on per unit mass property improvements.

A wide variety of functional TTR elements have been explored with respect to sensing. Zhang et al. [8] investigated the feasibility of measuring progressive delamination using through thickness electrical resistance in z-pinned composites. Martins et al. [17] investigated damage monitoring by the piezoresistive effect of the tufting threads in the sandwich structures. The commonality in these works is that they adapt the sensing technology to suit what can already be achieved using TTR. To expand this functionality more complex sensing systems should be applied, the geometry of which does not always satisfy the geometrical and mechanical constraints of existing TTR methods. This can be the case for photonic sensors but can be extended to include fluid flow channels and joining elements, where post-cure composite drilling is left as the only option for integrating these structures. Drilling is composites is undesirable and can cause problems with excessive failure under loading, splintering of fibres, delamination, burrs, microcracks, matrix burning and fibre peel-up [18].

The influence of the geometry (normally sub millimetre) and placement of TTR pins and their effects on the final mesoscale structure and macroscale properties has been extensively evaluated [19–21]; however, few studies have addressed the insertion process of TTR pins from a processing perspective with particular emphasis on the insertion forces experienced by the pin and on the quality of insertion [22–24]. Low insertion forces on the pin are desirable if delicate functional TTR elements are to be integrated. Furthermore, no studies are available that characterise the insertion process for pins that do not fall into the geometrical boundary limits of z-pinning i.e. pins with diameters greater than 1 mm. The motivation for this work is to address the need for TTR techniques that allow for the integration of much larger functional elements like fluid flow channels, thermal/electrical management elements, sensing assemblies, moulded-in fasteners, whose integration is currently outside the envelope of applicability of existing TTR methods.

This work investigates a new method for the direct insertion of large diameter TTR elements in prepreg based composite laminates. The focus here is on characterising the insertion process and identifying the key process parameters that influence the forces experienced by the pin during insertion and the quality of the insertion with respect to prepreg damage. A study into the thermal stability of the prepreg used in this work at elevated working temperatures is carried out to assess time limits of the application of moderate heating during insertion and identify a riskless processing window. This analysis sets the stage for a future investigation into the thermomechanical behaviour of the cured system (e.g. shrinkage and thermal stability). The effect of the pin leading edge and pin diameter is explained with reference to the pin-prepreg contact and insertion mechanics. The significance of preform consolidation state is evaluated for fully unconsolidated prepreg stacks and stacks under 1 bar of consolidation pressure simulating a debulked state.

## 2. Methodology

### 2.1. Materials and manufacturing

The prepreg system used in this work was 12 k (650 gsm) BX180-220 carbon-benzoxazine prepreg manufactured by SHD Composite Materials Ltd. [25]. The prepreg has a 2 × 2 twill weave with each cured ply of this material measuring 0.66 mm and a fibre volume fraction ($v_f$) of ~60%. This prepreg is specially designed for manufacturing composite tooling and was selected because of its low tack, low shrinkage, good thermal stability, extended out-life, and ease of handling. The properties of prepreg used in this study is highly desirable because the material is semi-rigid at room temperature [25,26], meaning that post-insertion cooling to room temperature fixes the TTR pins in place. The recommended cure cycle for this material is 2 h at 160 °C followed by 2 h at 180 °C under 6 bar autoclave pressure. Prepreg preform specimens were manufactured using 16-layers of BX180-220 with a layup consisting of equal amounts of plies oriented in the 0/90 and ±45° orientations.

Through-thickness reinforcing pins were manufactured from 304 stainless steel [27] rods with diameters of 1.2, 1.5 and 2.0 mm machined to a length of 25 mm. Either a 45° chamfer or a 45° conical point was machined into the leading edge of the rods to allow for parting of the prepreg tows in the preform (Fig. 1c).

Different leading edge (LE) geometries are in use for z-pins, tufting heads, and stitching needles, which all must facilitate the parting of the tows during insertion [28]. These LE geometries include but are not limited to chamfers/bevels, cones, tapers, ball points, with chamfers being the most common. The use of different LEs for these applications, and in more general puncture/penetration applications like tissue penetration for hypodermic needles, is heavily influenced by the trade-off between the loads involved in the specific application, the needle/pin size, pin life (single use or reusable) and machining costs. For example, in z-pins chamfered LEs are simple and cheap to machine on small (sub 1 mm diameter) rods, whereas ball points or cones are significantly more difficult and costly to achieve.

### 2.2. Characterisation of thermal ageing

Thermal ageing tests were carried out to investigate the thermal robustness of the prepreg material and to determine time limits of elevated temperature exposure during processing that do affect the advancement of curing in the material. Small sample plies (30 mm × 30 mm) of BX180-220 were placed in an oven at either 60 °C or 90 °C for between 2 and 16 h. Samples of 5–10 μg were then cut from aged prepreg specimens and analysed via Modulated Differential Scanning Calorimetry (MDSC) process using a TA Q200 DSC machine [29]. The thermal profile of the experiment consisted of a ramp from −30 °C to 60 °C at a rate of 2 °C/min with a modulation of ±1 °C/min to determine the glass transition temperature ($T_g$) of the prepreg.

### 2.3. Pin insertion trials

Through-thickness reinforcement insertion was carried out using a TA.HDplus Texture Analyser [30], which is a universal testing machine with a 1 kN load cell, a force resolution of 1 N and a displacement resolution of 0.001 mm. Fig. 1 shows the experimental setup of the insertion apparatus comprising the TA.HDplus Tex-

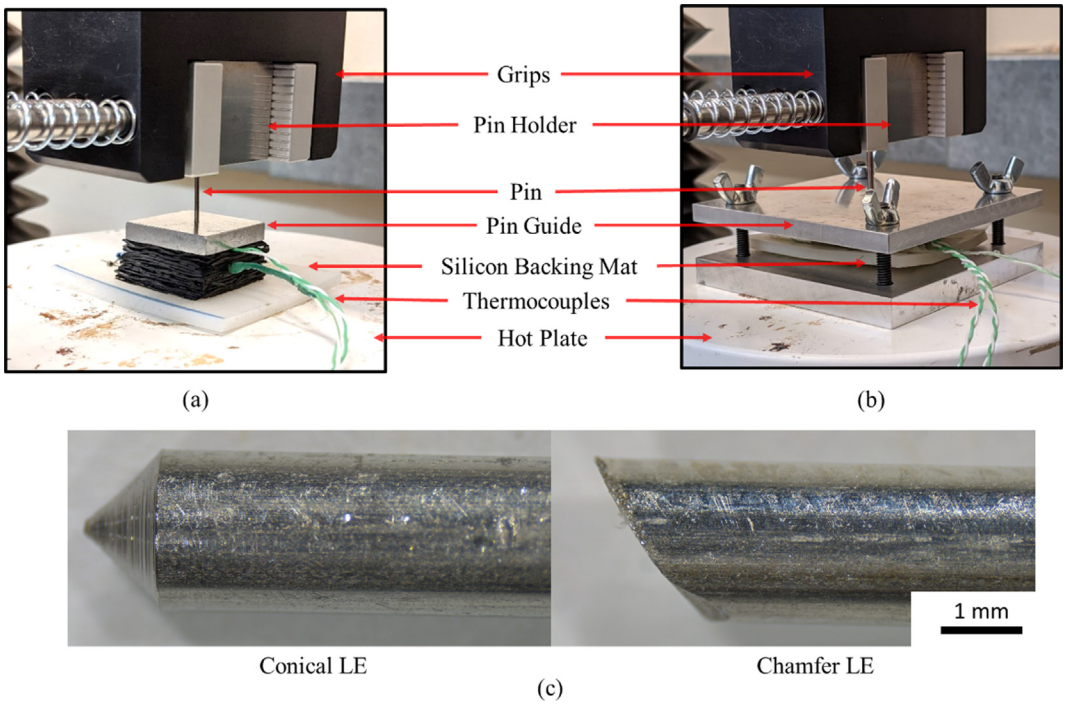


**Fig. 1.** Experimental setup for insertion characterization in (a) unconsolidated preforms, (b) consolidated preform and (c) showing leading edge geometry.

ture Analyser with a hot plate placed on the lower platen and a stainless-steel pin holder tightened between the upper grips. These pin holders were machined 25 mm × 25 mm × 25 mm stainless steel cubes with a 4 mm deep hole, in which the pins were placed, corresponding to the various pin sizes machined into one of the faces. A 60 mm × 60 mm × 3 mm square of 50 Shore hardness silicon, manufactured by JFlex [31] was placed between the hot plate and the preform to allow for penetration past the bottom prepreg layer. K-type thermocouples were placed at 3 locations in the preform: between the top surface of the backing silicone and the bottom layer of the preform, at the mid-layer of the preform, and between the top layer of the preform and the pin guide (Fig. 1a and b).

Prepreg stacks were cut and laid-up according to the specification in Section 2.2. Specimens were then wrapped in a single layer of release film and placed into an oven at 70 °C for at least 1 h or until all the thermocouples read a temperature between 60 and 80 °C. For insertion into unconsolidated stacks (Fig. 1a), specimens were then transferred to the silicone backing layer on the hot plate, which was maintained at 60 °C. A preheated guide plate (60 °C) was then place on top of the stack and the pin was placed into the guide plate hole. The top grip with the pin holder was then lowered to contact the back end of the pin. Once the pin alignment and stack temperatures were verified, the insertion was started with the pin insertion carried out at a fixed displacement rate of 0.5 mm/s for a fixed insertion depth of 13 mm, which was sufficient to penetrate the full prepreg stack and partially penetrate the silicone backing layer. Once insertion was completed, the upper grip was raised, leaving the pin lodged in the prepreg stack. For insertion into consolidated specimens (Fig. 1b), there was an additional consolidation step. Upon removal from the oven, specimens were transferred to a clamping fixture which applied a compression force equivalent to 1 bar consolidation pressure. To achieve this, a force of 90 N was applied by the upper platen of the TA.HDplus device followed by fastening of the wing nuts of the fixture at the displacement level attained on loading. Once the alignment and temperatures were verified, the insertion started with the pin being inserted in a similar way as in unconsolidated specimens, but instead with a fixed insertion depth of 10 mm in this case as the consolidated sample is thinner. Between 3 and 5 insertion tests were carried out for each condition/case considered. Peak insertion force is defined as the maximum force registered by the load cell between the start of insertion and the full insertion depth, ignoring any artificial load recovery resulting from the transition between the prepreg and the silicone backing layer.

### 2.4. Specimen post-processing and analysis

For optical microscopy, specimens were first cured either free-standing (unconsolidated samples) or in the consolidation jig (consolidated samples) for 2 h at 160 °C followed by 2 h at 180 °C in an oven. These samples were then set in a small resin filled pot to preserve the geometry and allow for the polishing of the cross-section for optical microscopy. Micro-CT scans were carried out on uncured specimens and images were obtained using a Nikon Metrology XT H225 micro-CT scanner.

## 3. Results and discussion

### 3.1. Thermal ageing

The BX180-220 prepreg is marketed as having excellent handleability in warm conditions being semi-rigid at room temperature (20–23 °C), with very low tack [25,32]. As a result, insertion through the prepreg is not possible at room temperature. The thermosetting matrix in prepregs is characterized by a state in which the material is partially but very sparingly crosslinked (cured), and viscosity and tackiness are elevated [33]. The viscosity of the prepreg matrix resin is a function of the temperature following an Arrhenius dependence. In the case of the benzoxazine matrix used here, heating of the material is required to sufficiently reduce its viscosity and allow relaxation and free movement of the tows in

order to insert pins through prepreg stack. Heating prepregs during pre-processing is an established forming procedure but data is currently unavailable on suitable pre-processing temperatures for BX180-220, necessitating investigation of its thermal stability. The benzoxazine prepreg used here is a relatively new material of a relatively new material class for the composites industry and data for of this kind for the material is not widely available. Working at a temperature where the material starts curing would render the process infeasible in an industrial context, so the role of this part of the work is to establish that the temperature required for insertion is acceptable.

The insertion process, although quick in practice, may require a lengthy heating process and dwell to equilibrate temperature through the stack thickness if a larger component with multiple insertion points is to be manufactured. The prepreg resin glass transition temperature ($T_g$) is closely correlated to the degree of cure, with $T_g$ increasing with crosslinking density [34]. The change in $T_g$ due to thermal ageing is used here as a metric of how prolonged exposure to working temperatures affects pre-curing to minimize the possibility of decreasing the viscosity of the system during insertion with adverse effects in subsequent steps of processing such as consolidation. The $T_g$ of the BX180-220 prepreg before any ageing determined using MDSC is 11.6 °C which is in line with the findings of Bornosuz et al. [32]. A working temperature starting around 50 °C above this value was selected as a suitable insertion temperature (60 °C) with an upper limit of 90 °C, where the prepreg stack and insertion apparatus are still easily handled without the need for extensive thermal protection by an operator. The range is also typical of current industrial hot forming processes for prepregs like in diaphragm forming [35] and corresponds to a suitable processing region (80–130 °C [32]) for benzoxazines in which the viscosity begins to reduce significantly [36].

Fig. 2 and Fig. 3 show the reversing heat versus temperature for samples aged at 60 °C and 90 °C for 2, 4, 8 and 16 h, on which the $T_g$ is manifested as a step due to the increase in heat capacity of the material upon the glass transition. The $T_g$ values are also summarised in Fig. 4. Fig. 2 and Fig. 4 show no significant change in the $T_g$ for the 2- and 4-hour ageing regimes at 60 °C. When samples are subjected to extended aging times of 8 and 16 h, the $T_g$ increases by just over 1 °C to a maximum of 12.6 °C. For the 90 °C ageing regime, Fig. 3 and Fig. 4 show a gradual increase in $T_g$ up to a maximum of 16.8 °C after ageing for 16 h. This increase in $T_g$ suggests that ageing at 90 °C does slightly advance the pre-cure state in the material. Typically, this small change in $T_g$, and by extension degree of cure, does not interfere with further material processing. In this small-scale experiment, 60 °C is sufficient to facilitate insertion and does not require extended times at elevated temperatures, but a greater temperature up to 90 °C can be considered in full scale manufacturing processes if necessary. The time the material in the following sections spends in an elevated temperature environment is typically between 1 and 2 h and is determined by the time at which internal thermocouples register a temperature above 70 °C (10 °C allowance for cooling during transference from the oven to a heated work surface).

### 3.2. Pin insertion

Fig. 5 compares typical force versus displacement curves for insertions with chamfered and conical LEs in unconsolidated stacks. Insertion curves generally follow a two-phase insertion profile in which curves are characterised by two distinct phases: the prepreg compression stage, and the steady-state crack propagation stage [23,24,37]. Fig. 6 shows mechanics of the insertion process. In the prepreg compression stage, the tip of the pin presses against the material surface and, instead of instantaneously parting the fibres, the prepreg layers compress locally under the force of the pin (Fig. 6a). This stage is defined by either a linear or non-linear increase in load up to a peak. At the peak, the stresses in the prepreg reach some critical value which then initiates through-thickness crack propagation in the form of tow parting (Fig. 6b), sometimes referred to as cutting. For the purposes of this paper, parting refers to the parting of tows without fracturing of the individual fibres, whereas cutting refers to individual fibre fracture resulting from being sliced or torn by the pin. The stage after the peak is defined as the steady-state crack propagation stage and is characterised by a small reduction in the load and is typically followed by load sustainment. Serrations in the curves are typically caused by friction between the pin and the material or by a build-up of force as the pin punctures a new layer of the prepreg stack.

The contact behaviour during insertion is governed by three force contributions which are important for understanding what contributes to changes in the overall insertion forces. In the prepreg compression stage, there is an initial point contact between the prepreg and the pin, meaning that the contributing force is a result of the through-thickness compression stiffness of the pre-

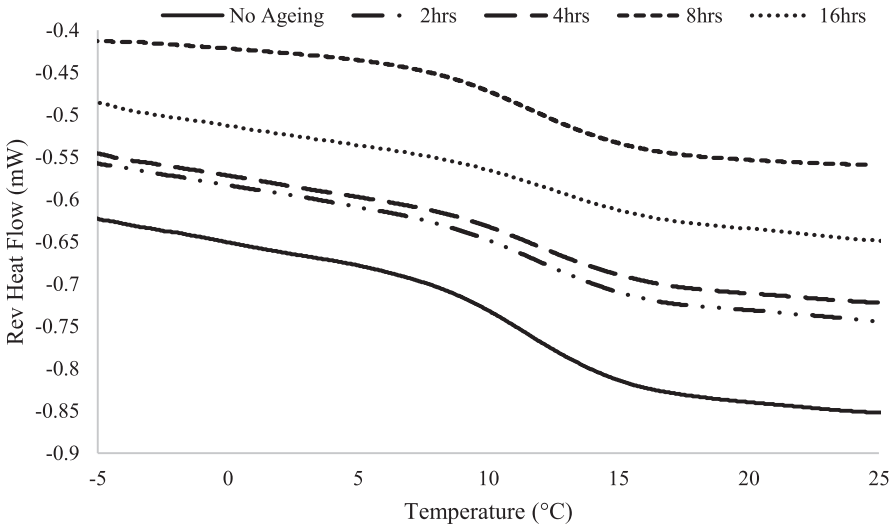


**Fig. 2.** Reversing heat flow versus temperature for thermal ageing tests conducted at 60 °C.

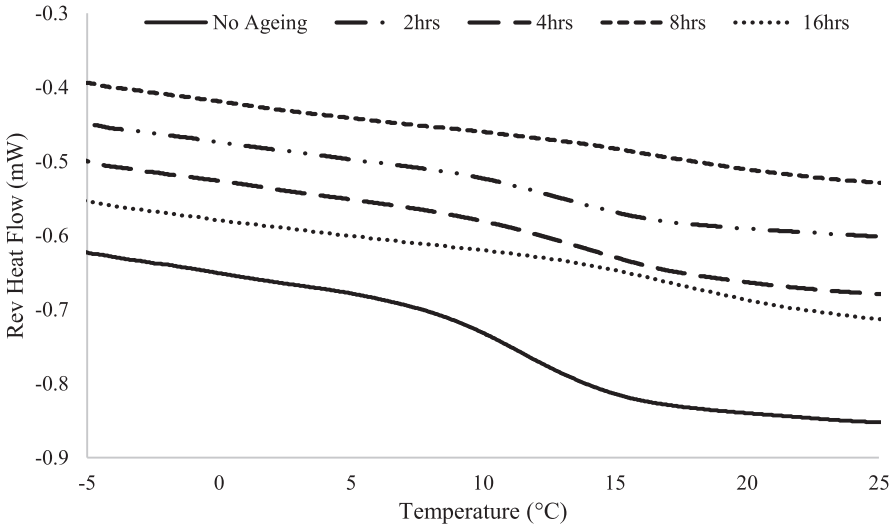


**Fig. 3.** Reversing heat flow versus temperature for thermal ageing tests conducted at 90 °C.

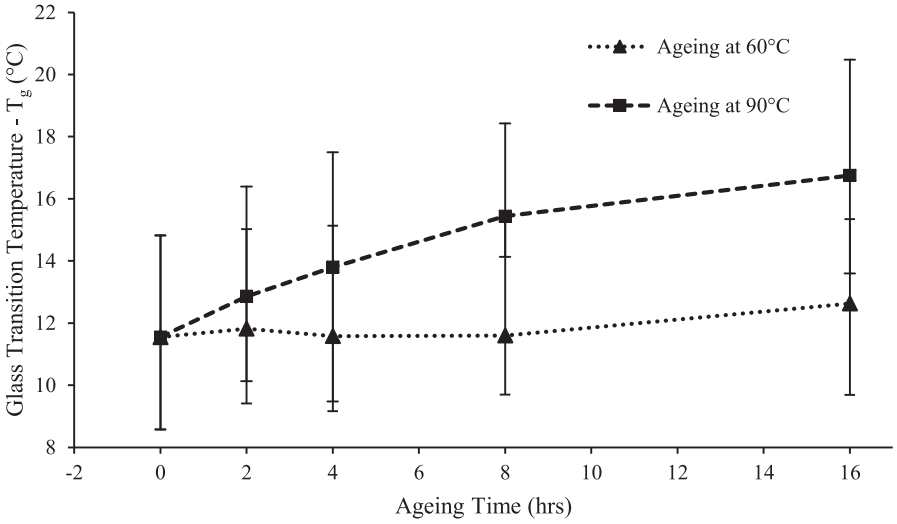


**Fig. 4.** Graph showing relationship between $T_g$ and ageing time at 60 °C and 90 °C.

preg only. This is referred to as the compression force ($F_c$). In the steady state crack propagation phase, there are three constituent forces that contribute to the total insertion force: the friction force ($F_f$), the parting force ($F_p$) and the extrusion force ($F_e$). Fig. 6c, shows the location and orientation of these forces.

Insertion in unconsolidated chamfered LE pins (Fig. 5) follows the two-phase load profile. This is characterised by an initial non-liner increase to a peak after which steady-state crack propagation ensues with a minor but noticeable upward trend in both ø1.2 mm and ø1.5 mm pin insertions. The value and location of the actual peak insertion force varies with pin diameter. The average peak insertion force in ø1.2 mm diameter pins is 6.1 N and peak insertion forces are located near the end of the insertion event at around 12–13 mm pin displacement. This increases by 143% to 14.9 N in ø1.5 mm pins, where peak insertion forces are similarly located near the end of the insertion event. This then increases by a further 141% to 35.9 N in ø2.0 mm pins, where the peak insertion forces are located at the initial peak ahead of steady-state crack propagation, between 5 mm and 10 mm pin displacement.

Insertion in unconsolidated conical LE specimens (Fig. 5) follows a different typical load profile. Instead of two distinct phases, there is just one which is characterised by a steady linear increase in load through the entire insertion event to a peak near the end of the insertion, typically around 12 mm to13 mm pin displacement, where the load increases as the pin crosses the threshold into the backing silicone layer. As pin diameter increases, the average slope of these curves increases from 0.1 N/mm in ø1.2 mm, to 0.13 N/mm in ø1.5 mm, and to 0.39 N/mm in ø2.0 mm diameter pins. Peak forces increase by 57% from ø1.2 mm to ø1.5 mm pins, and by a further 124% from ø1.5 mm to ø2.0 mm pins. Comparing micro-CT images of chamfer LE (Fig. 7a) to conical LE (Fig. 7c) ø2.0 mm pins, conical LE pins show better insertion with little out of plane tow deviation, suggesting that the conical LE is more efficient at parting tows early in the insertion process with minimal prepreg compression and associated local distortion. This phenomenon has been observed in ø1.2 mm pins, with increasing frequency in ø1.5 mm pins, but happens every time in ø2.0 mm pins. Distortions become worse with increasing pin diameter but in ø1.2 mm and

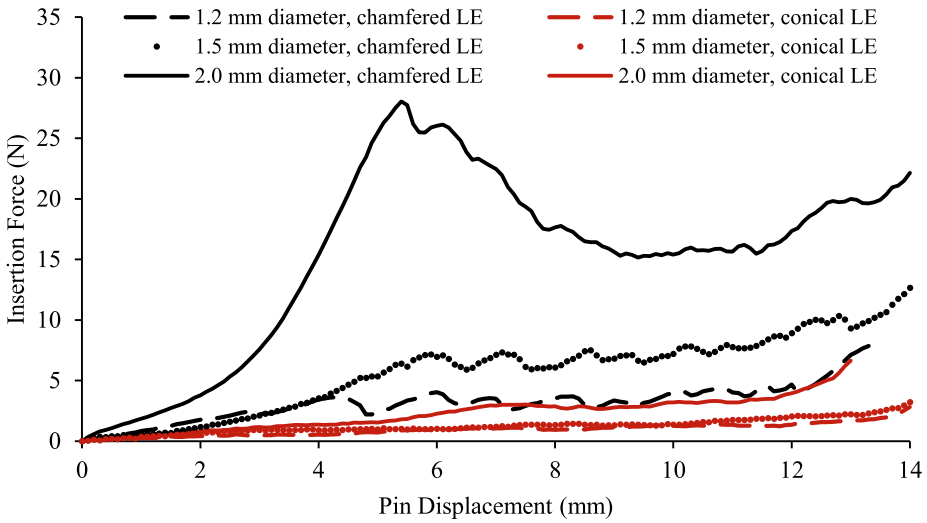


**Fig. 5.** Insertion force vs. pin displacement for unconsolidated preform.

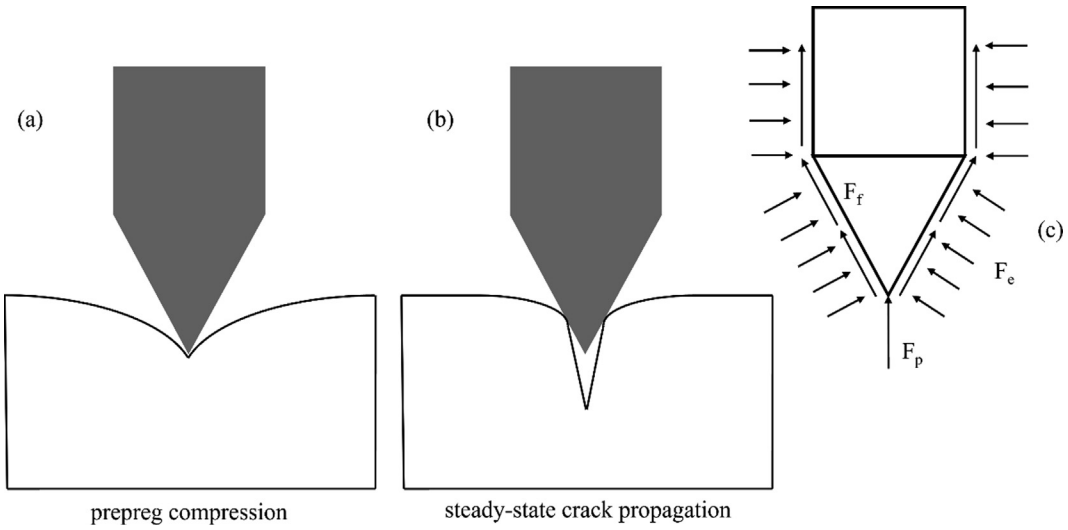


**Fig. 6.** Diagrammatic representation of (a) prepreg compression, (b) steady-state crack propagation, and (c) constituent insertion forces during the pin insertion process.

ø1.5 mm pins, the layers can recover after being cut by the chamfered LE (Fig. 7e and f). In ø2.0 mm pins, the distortion is so severe that the tows cannot rearrange themselves around the pin and extensive distortion occurs Fig. 7a.

Fig. 8 illustrates typical force versus displacement curves for insertion in consolidated stacks. Chamfered and conical LEs behave more similarly in consolidated stacks, abiding by the two-phase behaviour expected in which there is a distinct prepreg compression and a steady state propagation stage. Prepreg consolidation has the effect of removing the non-linearity in the initial load rise in the chamfered LE insertion, which is associated with prepreg compression, and both LEs exhibit similar initial slopes. The average initial slopes are 4.1 N/mm and 5.3 N/mm for ø1.2 mm pins, 4.0 N/mm, and 5.0 N/mm for ø1.5 mm pins, and 14.1 N/mm and 13.8 N/mm for ø2.0 mm pins for the chamfered and conical pins respectively. In the consolidated state for chamfered LE pins, peak forces increased by 115% from ø1.2 mm to ø1.5 mm pins, and by a further 166% from ø1.5 mm to ø2.0 mm pins. In conical LE pins peak forces increased by 95% from ø1.2 mm to ø1.5 mm pins, and by a further 141% from ø1.5 mm to ø2.0 mm pins. In this case, the force required for local compression of the stack far exceeds the force required to either part or cut the tows, resulting in good quality insertions with small distortion zones in both cases (Fig. 7c and d). In both chamfered and conical LE pins, there is no clear trend with respect to the location of the peak insertion force, likely due to the greater influence of the silicone backing layer in the later stages of insertion, which could cause and artificial load rise. Additionally, it is difficult to judge the transition between the prepreg stack and the silicone backing layer in these consolidated tests.

The results reported in Fig. 9 show the variation of peak insertion force with pin diameter and suggest an exponential relationship between pin diameter and peak insertion forces. The points represent mean values for peak insertion force and the trendlines represent an exponential model using a least squares method for data fitting. The model is:

$$F(d) = C^{\alpha d} \tag{1}$$

where F is the peak insertion force in Newtons, d is the pin diameter in millimetres and C and α are coefficients of the exponential fitting.

The slope of the log curves for chamfered LE pins (α) is 2.2 $mm^{-1}$ for both consolidation states; and the slope of the log curves for conical LE pins is 1.6 $mm^{-1}$ and 1.9 $mm^{-1}$ for the unconsolidated and consolidated states respectively. This suggests a

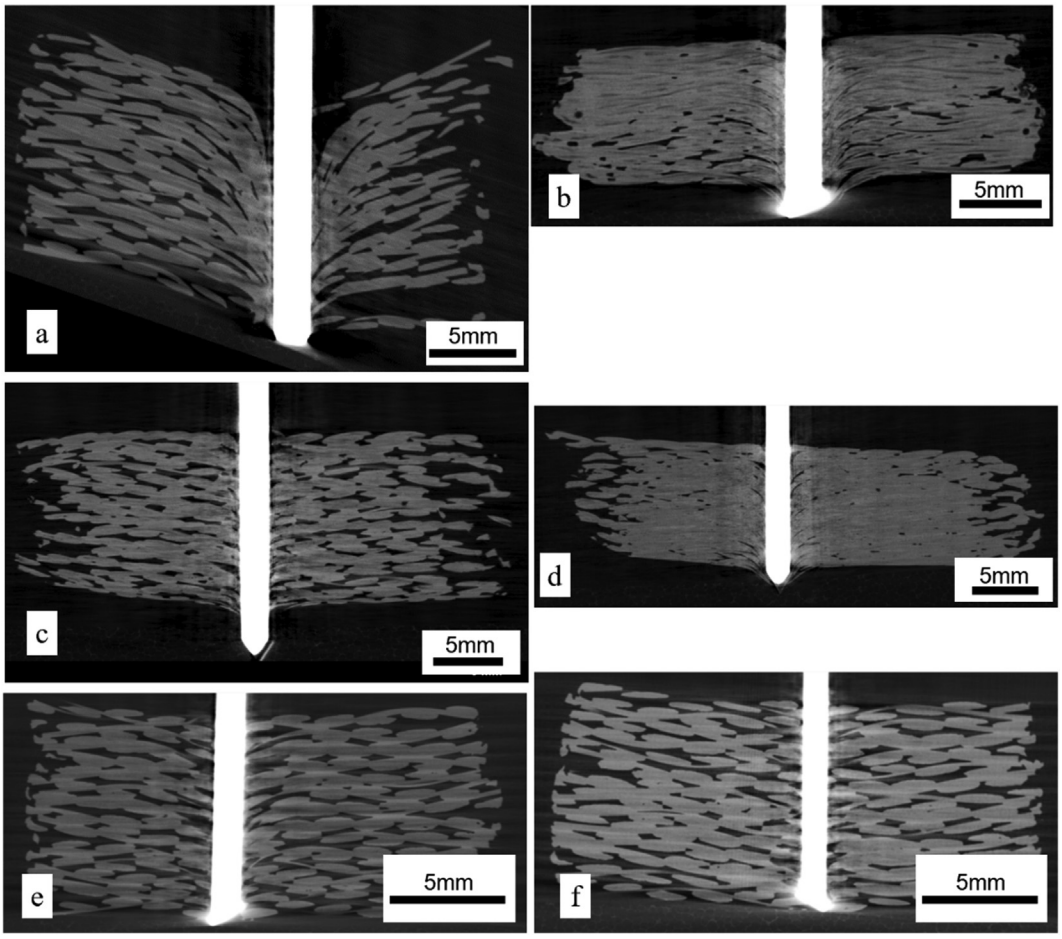


**Fig. 7.** Micro-CT images of inserted samples with ø2.0 mm pins (a–d) showing (a) chamfered LE in unconsolidated sample, (b) conical LE in unconsolidated sample, (c) chamfered LE in consolidated sample, (d) conical LE in consolidated sample, and (e) ø1.5 mm and (f) ø1.2 mm pins showing chamfered LE in unconsolidated samples.

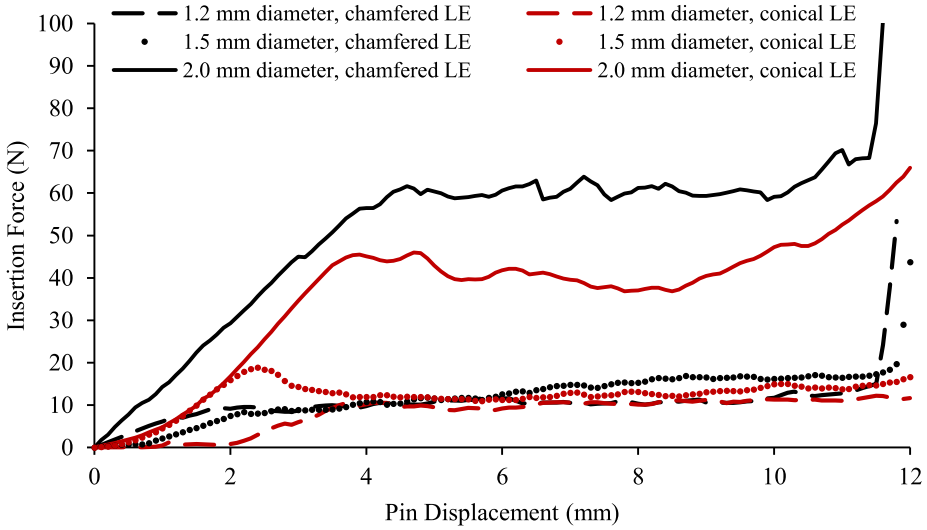


**Fig. 8.** Insertion force vs. pin displacement for consolidated preform.

dependence of the slope on the LE type. The exponential trendlines also show that the average peak forces in chamfered LE insertions exceed that of conical LE insertions. This is attributed to the fact that chamfered LEs are generally less efficient at parting tows, instead resulting in significant prepreg compression, tow snagging, and cutting during both the insertion phases (Fig. 7a). Although similar studies on LE effects are not available for prepreg insertion, comparisons can be made with similar work on needle insertion in biological materials. Okamura et al. [38] and Mavash and Dupont [37] investigated the effect of needle LE on insertion forces for a

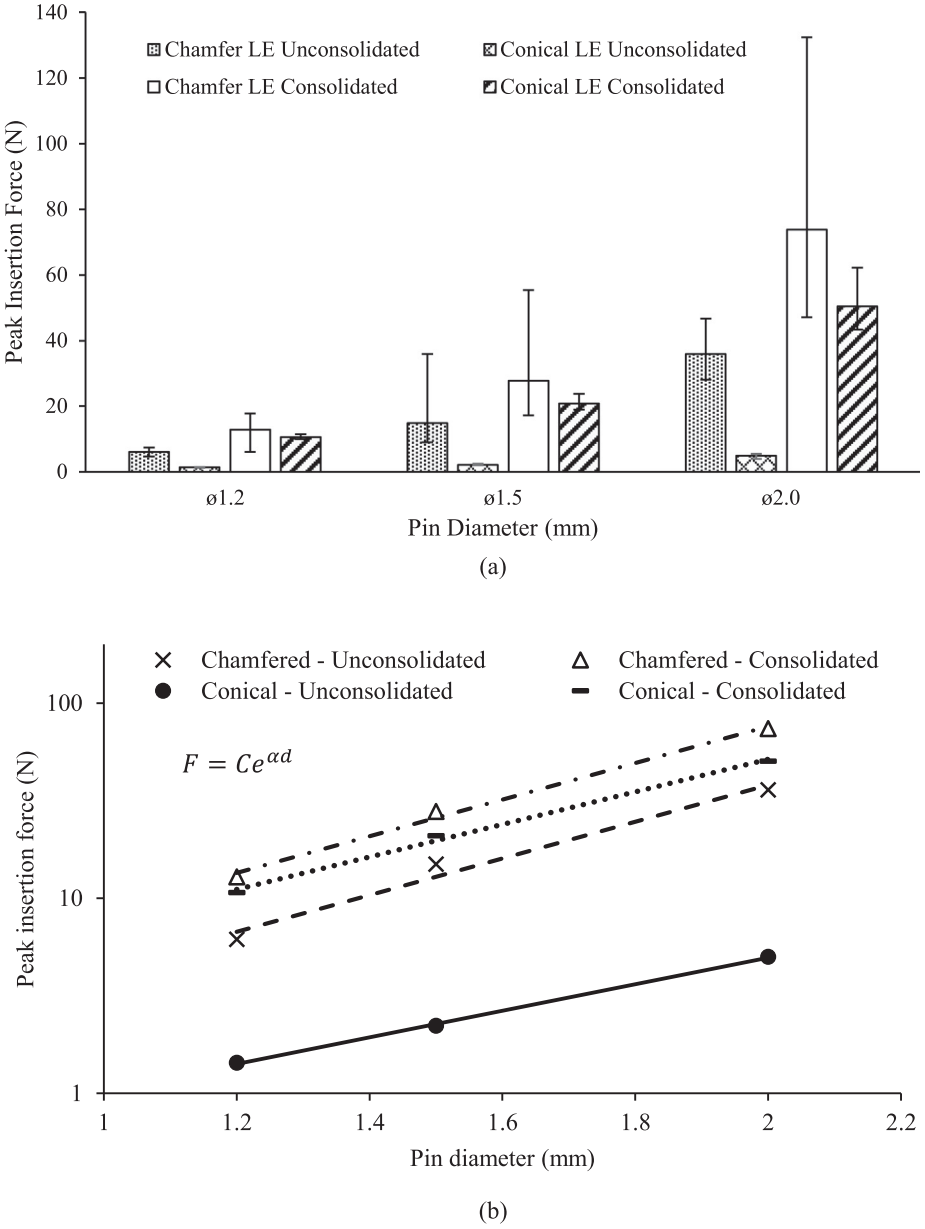


**Fig. 9.** Variation of peak insertion forces with respect to pin diameter on (a) linear scale and (b) logarithmic scale.

series of bevelled (chamfered), conical, triangular, and trocar tipped needles inserted into biological tissue and observed similar increases in both the initial slope and peak forces.

There is a much larger variation in peak force results in chamfered LE insertions (Fig. 9a), with a variation range of 16–70% compared with 7–13% in conical LE pins. This is due to the non-symmetric nature of the chamfered leading edge, meaning that insertion forces are dependent on the orientation of the LE with respect to the tow it is interacting with. This dictates whether the LE will part (lower force) or compress then potentially cut (higher force) the tow. On a mesoscopic and microscopic scale, the material is highly anisotropic, and the fracture stress of a tow or fibre is highly dependent on the principal stress direction. In the event where the tip of the chamfer aligns with the tow direction, tow splitting occurs along the tow axis and is defined by the transverse failure stress in the tow, which is negligible for a tow which can be considered loose in the case were the matrix is uncured and in the liquid state. However, if the chamfer tip aligns transversely to the tow direction, there is no sonication like in z-pinning [15] to perturb the individual fibres out of the path of the pin tip. In this case, the compression of the prepreg stack under the force of the pin results in local tensile stresses in the tow along the principal direction. This results in fracture of a portion of the fibres in the tow, which is reflected by increased insertion forces. This is like observations by Verma et al. [28], where laminate damage during tufting was found to be highly dependent on the needle tip geometry and was less pronounced where needle tips were symmetrical. Furthermore, in the work by Verma et al. [28], more through-thickness damage, like tow dragging, in unsymmetrical needles and a similar relationship between the needle tip orientation and the primary tow direction were observed. This interaction depends on the combination of pin diameter, tow size, orientation of the tow, and consolidation state.

As pin diameter increases, there is a non-linear increase in peak insertion force (Fig. 9b) with a higher rate of increase in chamfered LE pins, where the slope of the log curves is steeper, than in conical

LE pins. Peak forces are typically near the end of the insertion in conical LE pins and earlier onset in chamfer LE pins as the pin diameter increases in unconsolidated insertions because of the large $F_c$ needed to initiate steady-state crack propagation in this case. However, there is no clear trend observed in the consolidated material because of the greater influence of the silicone backing layer. This non-linear increase in insertion force is despite a linear increase in pin diameter and pin circumference, increasing by 25% from ø1.2 mm to ø1.5 mm pins, and by a further 33 % from ø1.5 mm to ø2.0 mm pins. There are two mechanisms by which this increase is achieved between the two insertion phases. In the prepreg compression phase, $F_c$ increases significantly as the insertion force is spread out over a larger cross-sectional area, resulting in greater initial compression than parting. This affects chamfered LE pins more severely as this is exacerbated by their inability to part fibres efficiently. In the steady state crack propagation phase, both the pin diameter and pin circumference are significant in evaluating the increase in insertion forces.

Optical microscopy images in Fig. 10 show the in-plane tow for specimens with varying pin diameters. Larger pins diameters displace a greater number of fibres to allow insertion and the increased pin circumference increases the contact area between the pin and the prepreg. No large lenticular shaped resin rich areas are noted even for the largest diameter pin insertion (Fig. 10c), which is typical of pins in UD architectures, which enhance pin-tow contact. These changes significantly increase $F_e$ (pin diameter dependent) and $F_f$ ($F_e$ and circumference dependent). There is a general assumption that $F_p$ is predominantly a function of pin LE geometry and preform consolidation state and is constant and independent of insertion depth [24].

The results reported here partially compare well with the findings of Cheng et al. [24], Ji et al. [23] and Wang et al. [22] where similar increases were noted and attributed mainly to increases in extrusion ($F_e$) and friction ($F_f$) forces. These works did not report large increases in $F_c$ probably because of the use of much smaller pins (~0.75 mm). Additionally, the effect was investigated for UD and cross ply laminates in these works. In a UD and cross ply laminates, the contact mechanism is such that only two sides of the lenticular shaped tow deformation path in any given layer are in contact with the pin (Fig. 11a). As the pin diameter increases, this contact interface increases, but not as significantly as in woven preforms, where the constraining of in-plane tow deformation caused by the woven weave architecture results in much greater pin-tow contact area (Fig. 11b). This drastically increases $F_e$ and $F_s$ more significantly than in UD laminates.

The magnitude of the increase in peak forces is also highly dependent on the consolidation state of the material. Consolidation packs tows together more tightly and because of more constrained tow movement along with increased inter-tow friction, greater force is required to part the tows ($F_p$), tows apply more extrusion force on the pin face ($F_e$) and higher contact forces from $F_e$ increase friction forces ($F_f$). The consolidation state of the prepreg preform was varied in these experiments between no consolidation and 1 bar of consolidation pressure, which is typical of the debulking phase of prepreg processing. These two states represent the boundaries of the envelope in which insertion is likely to take place.

The curves in Fig. 5 and Fig. 8 which compare typical force–displacement curves for unconsolidated and consolidated tests respectively, display clear trends that differentiate the two consolidation state scenarios. Consolidated insertions typically have greater insertion forces and a more stable crack propagation stage due to greater homogeneity, whereas forces in unconsolidated specimens tend upwards in the crack propagation phase. This is likely because local prepreg compression in the layers below the advancing crack tip as the pin approaches the silicone backing layer below. In this case, the $F_c$ of the silicone (~35 N for ø2.0 mm pin with conical LE) is higher than the $F_c$ of the prepreg which leads to a load increase approaching the transition point between the prepreg and the backing silicone in unconsolidated preforms. This is not true of ø2.0 mm chamfer LE pins, where the LE geometry causes significant local prepreg compression. Additionally, the onset of crack propagation is expedited in consolidated samples because the material is pre-compressed, meaning that the critical stress required to transition to the steady state crack propagation stage is achieved sooner.

As shown in micro-CT images in Fig. 7a, tow snagging is observed with significant out of plane deviation of tows that are effectively dragged downward through the preform starting in the prepreg compression stage resulting in a large tow deformation zone. This dragging and bunching of tows, caused by the inefficient tow parting in chamfered LE specimens, is responsible for a build-up of preform resistance ($F_c$) and hence insertion forces. This phenomenon is not present in Fig. 7b, where conical LE specimens are shown to penetrate unconsolidated specimens without this tow snagging and bunching issue. More efficient parting of the conical LE results in a smaller tow deformation zone and lower insertion forces. Consolidated samples seem to show similar cross-sections regardless of LE type in Fig. 7c and d, with similarly small tow deformation zones. The added consolidation in the prepreg stack provides some resistance to movement of the fibres in the z-direction meaning that even if fibres are snagged, there is significant backing pressure on the tow to encourage a tow to be cut, rather than be dragged downwards.

In the case of conical pins, consolidation state does not seem to significantly affect the quality of the insertion and a low or no consolidation approach can be taken if lower insertion forces are prioritized. The same cannot be said for chamfered LE specimens

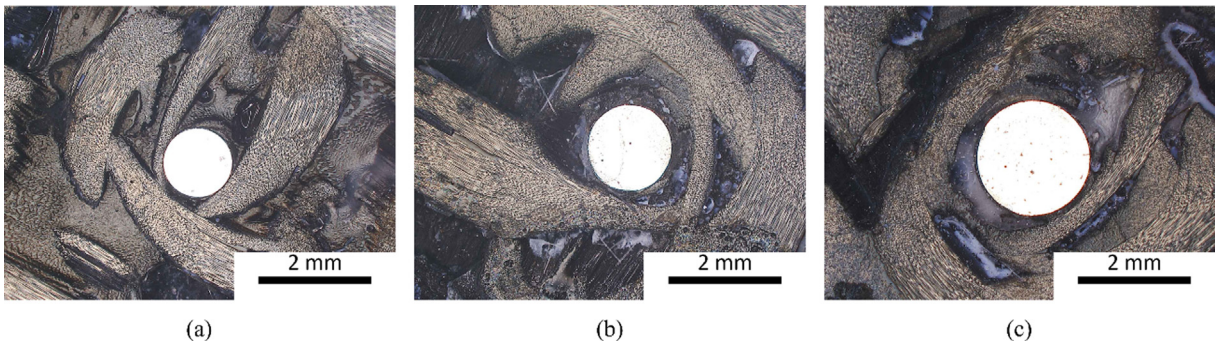


**Fig. 10.** Optical microscopy images showing the in-plane tow deviation around (a) ø1.2 mm, (b) ø1.5 mm, and (c) ø2.0 mm pins inserted in unconsolidated specimens.

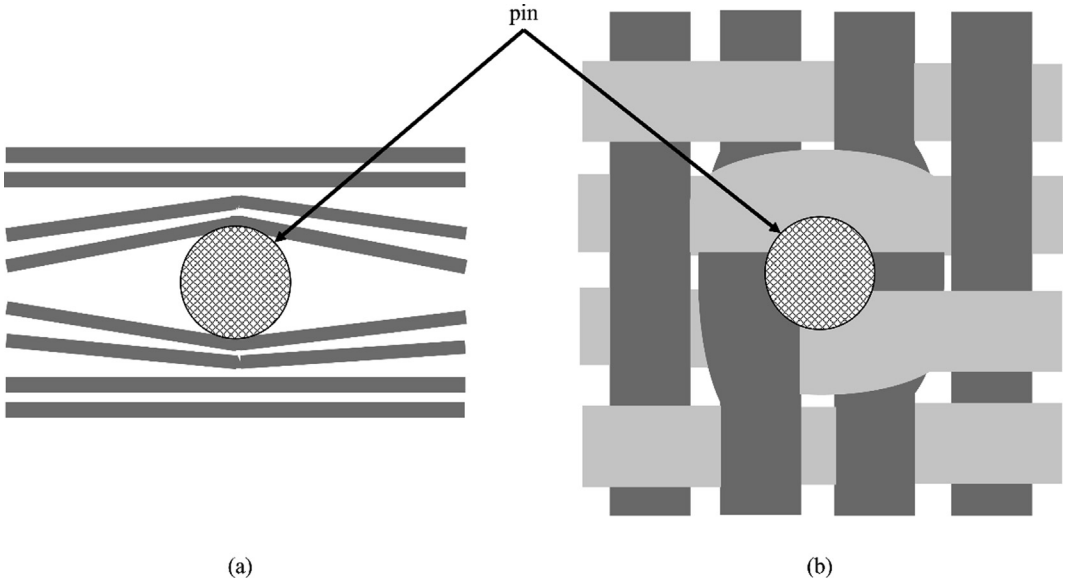


**Fig. 11.** Schematic of tow-pin contact in (a) unidirectional; and (b) woven architectures.

where consolidation state plays a major role in determining the quality of the insertion in terms of the size of the tow affected zone and damage to the tows.

## 4. Conclusion

This work identified conditions and a setup that allows insertion of large diameter pins into prepreg stacks. Pins of diameter between 1.2 mm and 2.0 mm are held in a bespoke pin holder and inserted at a constant speed using into prepreg stacks, which are heated to 60 °C to allow more free movement of the tows. For the material investigated here, thermal ageing experiments show no significant change in $T_g$, and by extension the degree of cure, after being held at 60 °C for up to 16 h. There is a small increase in $T_g$ in the prepreg after being held at 90 °C for longer than 4 h. However, insertion could be carried out at the higher temperature point for up to 4 h without much change in the degree of cure. Pin insertion in this study takes place at 60 °C for about 2 h and has no real effect on advancing the degree of cure in the material.

The pin leading edge geometry has shown a marked effect on the insertion process. As expected, conical pins induce lower peak forces than chamfered pins during insertion and show more repeatable results with more steady force–displacement curves. Chamfered leading edge pins are less efficient tow parting and their behaviour is highly dependent on the relationship between the orientation of the pin and the tow it is interacting with. Increasing the pin diameter has the effect of increasing the insertion forces required, primarily because of increased compression in the prepreg compression stage and increased extrusion and friction forces in the steady state crack propagation stage. This increase is most pronounced in chamfered leading-edge pins where the poor efficiency of tow parting combined higher extrusion forces results in much higher forces. Preform consolidation increases the insertion forces but is also highly dependent on the leading-edge geometry. However, consolidation has the effect of significantly improving the quality in terms of reducing damage and tow distortions. This has a more marked effect in chamfered leading edge pins experiments.

This work demonstrated that the insertion of large diameter pins, far exceeding the capabilities of current TTR methods, is possible in prepreg stacks with low insertion forces acting on the pins and minimal disruption to tow architecture. Further investigations are needed to expand the envelope of applicability to even larger diameter pins and to better understand the parameters that affect insertion forces and quality, namely tow size, weave architecture, and leading-edge geometry. Simultaneously, the intricacies of the insertion contact mechanics can be explored through the development of predictive methods. The effect of the embedded pin on cured composite properties, namely mechanical performance (in-plane and out-of-plane), thermomechanical properties, shrinkage and part quality will be explored in future. Innovations are needed to develop bespoke equipment capable of reliably performing pin insertions with the potential for scaling up to multi-pin insertion. This technology can be applied for the integration of large diameter multifunctional elements, joining applications, and the more efficient integration of moulded-in holes.

## CRediT authorship contribution statement

**Geoffrey Neale:** Conceptualization, Methodology, Validation, Formal analysis, Investigation, Data curation, Writing – original draft, Writing – review & editing, Visualization, Project administration. **Alex Skordos:** Conceptualization, Methodology, Formal analysis, Data curation, Writing – review & editing, Visualization, Project administration, Funding acquisition.

## Declaration of Competing Interest

The authors declare that they have no known competing financial interests or personal relationships that could have appeared to influence the work reported in this paper.

## Acknowledgements

This work was supported by the SEER project which has received funding from the European Union's Horizon 2020 research and innovation programme (Grant agreement 871875).

## Data availability statement

The raw data underlying this study can be accessed through the Cranfield University repository at https://doi.org/10.17862/cranfield.rd.17069717 [dataset] [39].

## References


[1] E.P. Koumoulos, A.-F. Trompeta, R.-M. Santos, M. Martins, C.M.D. Santos, V. Iglesias, R. Böhm, G. Gong, A. Chiminelli, I. Verpoest, P. Kiekens, C.A. Charitidis, Research and development in carbon fibers and advanced high-performance composites supply chain in Europe: A roadmap for challenges and the industrial uptake, J. Compos. Sci. 3 (3) (2019) 86.

[2] I.K. Partridge, D.D.R. Cartié, Delamination resistant laminates by Z-Fiber® pinning: Part I manufacture and fracture performance, Compos. Part A: Appl. Sci. Manuf. 36 (2005) 55–64, https://doi.org/10.1016/j.compositesa.2004.06.029.

[3] K.A. Dransfield, L.K. Jain, Y.W. Mai, On the effects of stitching in CFRPs—I. mode I delamination toughness, Compos. Sci. Technol. 58 (1998) 815–827, https://doi.org/10.1016/S0266-3538(97)00229-7.

[4] K. Grigoriou, R.B. Ladani, A.P. Mouritz, Electrical properties of multifunctional Z-pinned sandwich composites, Compos. Sci. Technol. 170 (2019) 60–69, https://doi.org/10.1016/j.compscitech.2018.11.030.

[5] F. Pegorin, K. Pingkarawat, A.P. Mouritz, Controlling the electrical conductivity of fibre-polymer composites using z-pins, Compos. Sci. Technol. 150 (2017) 167–173, https://doi.org/10.1016/j.compscitech.2017.07.018.

[6] C. O'Keeffe, L.R. Pickard, J. Cao, G. Allegri, I.K. Partridge, D.S. Ivanov, Multi-material braids for multifunctional laminates: conductive through-thickness reinforcement, Funct. Compos. Mater. 2 (2021), https://doi.org/10.1186/s42252-021-00018-0.

[7] D.M. Lombetti, A.A. Skordos, Lightning strike and delamination performance of metal tufted carbon composites, Compos. Struct. 209 (2019) 694–699, https://doi.org/10.1016/j.compstruct.2018.11.005.

[8] B. Zhang, G. Allegri, S.R. Hallett, An experimental investigation into multi-functional Z-pinned composite laminates, Mater. Des. 108 (2016) 679–688, https://doi.org/10.1016/j.matdes.2016.07.035.

[9] T.M. Koh, S. Feih, A.P. Mouritz, Experimental determination of the structural properties and strengthening mechanisms of z-pinned composite T-joints, Compos. Struct. 93 (2011) 2222–2230, https://doi.org/10.1016/j.compstruct.2011.03.009.

[10] T. Löbel, B. Kolesnikov, S. Scheffler, A. Stahl, C. Hühne, Enhanced tensile strength of composite joints by using staple-like pins: Working principles and experimental validation, Compos. Struct. 106 (2013) 453–460, https://doi.org/10.1016/J.COMPSTRUCT.2013.06.020.

[11] A. Arnautov, A. Nasibullins, V. Gribniak, I. Blumbergs, M. Hauka, Experimental characterization of the properties of double-lap needled and hybrid joints of carbon/epoxy composites, Materials 8 (2015) 7578–7586, https://doi.org/10.3390/ma8115410.

[12] I. Gnaba, X. Legrand, P. Wang, D. Soulat, Through-the-thickness reinforcement for composite structures: a review, J. Ind. Text. 49 (2019) 71–96, https://doi.org/10.1177/1528083718772299.

[13] V. Kostopoulos, N. Sarantinos, S. Tsantzalis, Review of through-the-thickness reinforced z-pinned composites, J. Compos. Sci. 4 (2020) 31, https://doi.org/10.3390/jcs4010031.

[14] G. Dell'Anno, J.W.G. Treiber, I.K. Partridge, Manufacturing of composite parts reinforced through-thickness by tufting, Rob. Comput. Integr. Manuf. 37 (2016) 262–272, https://doi.org/10.1016/j.rcim.2015.04.004.

[15] A.P. Mouritz, Review of z-pinned composite laminates, Compos. A Appl. Sci. Manuf. 38 (2007) 2383–2397, https://doi.org/10.1016/j.compositesa.2007.08.016.

[16] N. Sarantinos, S. Tsantzalis, S. Ucsnik, V. Kostopoulos, Review of through-the-thickness reinforced composites in joints, Compos. Struct. 229 (2019) 111404.

[17] A.T. Martins, Z. Aboura, W. Harizi, A. Laksimi, K. Hamdi, Structural health monitoring by the piezoresistive response of tufted reinforcements in sandwich composite panels, Compos. Struct. 210 (2019) 109–117, https://doi.org/10.1016/j.compstruct.2018.11.032.

[18] A. Galińska, Mechanical joining of fibre reinforced polymer composites to metals—a review. Part I: bolted joining, Polymers 12 (2020) 2252, https://doi.org/10.3390/polym12102252.

[19] G. Pappas, S. Joncas, V. Michaud, J. Botsis, The influence of through-thickness reinforcement geometry and pattern on delamination of fiber-reinforced composites: Part II – Modeling, Compos. Struct. 181 (2017) 379–390, https://doi.org/10.1016/j.compstruct.2017.08.096.

[20] B. Najafloo, A.M. Rezadoust, M. Latifi, Effect of through-the-thickness areal density and yarn fineness on the mechanical performance of three-dimensional carbon-phenolic composites, J. Reinf. Plast. Compos. 35 (2016) 1447–1459, https://doi.org/10.1177/0731684416653839.

[21] G. Pappas, S. Joncas, V. Michaud, J. Botsis, The influence of through-thickness reinforcement geometry and pattern on delamination of fiber-reinforced composites: Part I - Experimental results, Compos. Struct. 184 (2018) 924–934, https://doi.org/10.1016/j.compstruct.2017.09.091.

[22] W. Wang, H. Wang, H. Wang, H. Dong, Y. Ke, Micro-damage initiation evaluation of z-pinned laminates based on a new three-dimension RVE model, Compos. Struct. 263 (2021) 113725.

[23] G. Ji, L. Cheng, S. Fei, J. Li, Y. Ke, A novel model of Z-pin insertion in prepreg based on fracture mechanics, Proc. Instit. Mech. Eng. Part B: J. Eng. Manuf. 235 (12) (2021) 1971–1982.

[24] L. Cheng, G. Ji, S. Fei, J. Li, Y. Ke, Analysis and modeling of the Z-pin insertion in prepreg based on contact mechanism, Polym. Compos. 42 (12) (2021) 6430–6441.

[25] SHD Composites, BX180-220 Benzoxazine Tooling Prepreg - Product Datasheet, (2017). https://shdcomposites.com/admin/resources/bx180-220-pds.pdf (accessed June 21, 2021).

[26] S. Rimdusit, C. Jubsilp, S. Tiptipakorn, Introduction to commercial benzoxazine and their unique properties, in: 2013: pp. 1–27. https://doi.org/10.1007/978-981-4451-76-5_1.

[27] Masteel UK Ltd., Grade 304H Stainless Steel (UNS S30409), (2019). https://www.azom.com/article.aspx?ArticleID=5050 (accessed July 8, 2021).

[28] K.K. Verma, G. Padmakara, K.M. Gaddikeri, S. Ramesh, S. Kumar, S. Bose, The key role of thread and needle selection towards 'through-thickness reinforcement' in tufted carbon fiber-epoxy laminates, Compos. B Eng. 174 (2019) 106970.

[29] TA Instruments, Differential Scanning Calorimetry (DSC) Q-series Discovery DSC2500 DSC250 DSC25, n.d.

[30] TA.HDplus Texture Analyser | Stable Micro Systems Products, (n.d.). https://www.stablemicrosystems.com/TAHDplus.html (accessed August 24, 2021).

[31] J-Flex, Silicone Sheets - J-Flex, (n.d.). https://www.j-flex.com/products/silicone-sheets-new/ (accessed October 15, 2021).

[32] N.V. Bornosuz, R.F. Korotkov, V.V. Shutov, I.S. Sirotin, I.Y. Gorbunova, Benzoxazine copolymers with mono- and difunctional epoxy active diluents with enhanced tackiness and reduced viscosity, J. Compos. Sci. 5 (9) (2021) 250.

[33] S. Rusnáková, M. Kalová, Z. Jonšta, Overview of production of pre-preg, prototype and testing, IOP Conf. Series: Mater. Sci. Eng. 448 (2018), https://doi.org/10.1088/1757-899X/448/1/012069 012069.

[34] L.K. Grunenfelder, S.R. Nutt, Prepreg age monitoring via differential scanning calorimetry, J. Reinf. Plast. Compos. 31 (2012) 295–302, https://doi.org/10.1177/0731684411431020.

[35] J. Sun, Y. Gu, M. Li, X. Ma, Z. Zhang, Effect of forming temperature on the quality of hot diaphragm formed C-shaped thermosetting composite laminates, J. Reinf. Plast. Compos. 31 (2012) 1074–1087, https://doi.org/10.1177/0731684412453778.

[36] S. Rimdusit, P. Jongvisuttisun, C. Jubsilp, W. Tanthapanichakoon, Highly processable ternary systems based on benzoxazine, epoxy, and phenolic resins for carbon fiber composite processing, J. Appl. Polym. Sci. 111 (2009) 1225–1234, https://doi.org/10.1002/app.29085.

[37] M. Mahvash, P.E. Dupont, Mechanics of dynamic needle insertion into a biological material, IEEE Trans. Biomed. Eng. 57 (2010) 934–943, https://doi.org/10.1109/TBME.2009.2036856.

[38] A.M. Okamura, C. Simone, M.D. O'Leary, Force modeling for needle insertion into soft tissue, IEEE Trans. Biomed. Eng. 51 (2004) 1707–1716, https://doi.org/10.1109/TBME.2004.831542.

[39] G. Neale, A. Skordos, Insertion of large diameter through-thickness metallic pins in composites: dataset, Cranfield Online Research Data Repository. (2022). https://doi.org/10.17862/cranfield.rd.17069717.